Supporting Information for

$NbSe_2$@PPy nanosheets as anode materials for flexible all-solid-state asymmetric supercapacitors

Guofen Song,[a,b‡*] Jinghan Li,[c‡] Changlin Dong,[a,c] Panpan Zhang,[a] Mengzhao Yang,[c] SangWook Park,[a] Tao Zhang,[a] Mingchao Wang,[a] Huanhuan Shi,[a] Qinglei Liu,[c*] Jiajun Gu,[c*] Xinliang Feng[a]

[a] Department of Chemistry and Food Chemistry & Center for Advancing Electronics Dresden, Technische Universität Dresden, Dresden 01062, Germany

[b] Shenzhen Institute of Advanced Technology, Chinese Academy of Sciences, Shenzhen 518055, P. R. China

[c] State Key Laboratory of Metal Matrix Composites, School of Materials Science and Engineering, Shanghai Jiao Tong University, Shanghai 200240, P. R. China

* Corresponding author. E-mail: gf.song@siat.ac.cn, liuqinglei@sjtu.edu.cn, gujiajun@sjtu.edu.cn

‡ These authors contributed equally to this work

Contents

Synthetic strategies

Chemicals

$NbCl_5$ (99 %), pyrrole (99%), oleylamine (OAM), ammonium persulphate ($(NH_4)_2S_2O_8$, APS), diazanium sulfate $(NH_4)_2SO_4$, polyvinyl alcohol (PVA), n-methyl-2-pyrrolidone (NMP), and lithium chloride (LiCl) were bought from Sigma-Aldrich. Manganese sulfate ($MnSO_4$), sodium nitrate ($NaNO_3$), Se powder (99 %), and graphite foil (0.13 mm, 99.8 %) were purchased from Alfa Aesar. All the solutions not specified were prepared using double-distilled water (ddH_2O). All of the chemicals are in analytical grade and used without further purification.

Synthesis of $NbSe_2$ nanosheets

The $NbSe_2$ nanosheets were synthesized in a one-pot reaction followed by thermal decomposition. In a typical reaction, 20 mL of degassed OAM was added to the mixture of $NbCl_5$ (1 mmol) and Se (2 mmol) in Ar. The mixture was vigorously stirred at the temperature of 250 °C for 4 h, during which the precursors dissolved and form a black suspension. The suspension was then cooled slowly (5 °C min^{-1}) from 250 °C to room temperature (RT) before being washed with hexane repeatedly. After dried in a vacuum, the air-stable intermediate is heated at 450 °C for 3 h in Ar.

Synthesis of $NbSe_2$@PPy (NPy-x) nanosheets

$NbSe_2$@PPy (NPy-x) nanocomposite was synthesized by the *in-situ* chemical oxidation polymerization on the surface of the $NbSe_2$ nanosheets. In a typical process, 80 mL $NbSe_2$ nanosheet solution (0.25 mg mL^{-1}) was mixed with different amounts of pyrrole monomers (25 µL, 50 µL, and 100 µL), followed by ultrasonication at RT. The solution is then transferred into an ice bath, cooled down to below 5 °C, and stirred for 30 min. The polymerization of pyrrole was induced by the dropwise addition of the APS solution and lasted for at least 12 h. 50 µL, 100 µL or 200 µL APS solution (0.41 g mL^{-1}) was added into the $NbSe_2$/pyrrole solution containing 25 µL, 50 µL or 100 µL pyrrole monomers, respectively (mole ratio of APS : pyrrole = 1 : 2). The product was collected by filtration, washed successively with ddH_2O and ethanol, and then dried at 60°C for 24 h in a vacuum to obtain black powder. For comparison, pure polypyrrole (PPy) was synthesized under the same condition in the absence of $NbSe_2$ nanosheets.

Synthesis of MnO_2 nanosheets

MnO_2 nanosheets were synthesized by a molten salt method.[1] Typically, 5 g of $NaNO_3$ was added into a crucible and transferred to the muffle furnace at a temperature of 350 °C for 10 min until it completely melted. 0.2 g of $MnSO_4$ powder was then added into the molten salt for 1 min. Then, the product was removed from the muffle furnace and cooled to RT at ambient conditions. Finally, the product was washed with ddH_2O to remove $NaNO_3$.

Synthesis of exfoliated graphene (EG)

EG was prepared by exfoliating graphite foils based on our previous work.[2,3] Typically, the exfoliation was performed in a two-electrode system, with the graphite foil as the working anode, the carbon rod as the counter electrode, and 0.5 M $(NH_4)_2SO_4$ as the electrolyte. The electrochemical exfoliation was carried out by applying a constant positive voltage (10 V) on the working electrode. The EG powder was first collected with cellulose filters and washed repeatedly with ddH_2O to clear any chemical residues. The EG powder was then dispersed in DMF by sonication for 2 h in an ice bath. The dispersion was kept for 24 h for the precipitation of un-exfoliated graphite flakes. The upper solution is collected for further use.

Preparation of working electrodes

Typically, the working electrodes were made by drop-casting the active material slurry on the surface of porous Ni foam and dried in a vacuum at 60 °C overnight. The slurries were prepared by mixing active materials with carbon black and PVDF at a mass ratio of 7.5 : 1.5 : 1 in NMP followed by ultrasonication for 0.5 h. The mass loading of the electrode is 1 mg cm^{-2}.

Asymmetric supercapacitor device assembly

EG was added to improve the flexibility of the electrodes. NPy-1 and MnO_2 were individually mixed with EG at the mass ratio of 1 : 1, followed by sonication in DMF for 2 h. NPy-1/EG and MnO_2/EG electrodes were obtained by vacuum filtration. The supercapacitor was assembled by simply sticking the two electrodes, separated by the cellulose membrane, after the drop-casting of PVA/LiCl gel electrolyte (prepared by dissolving 4 g PVA and 8.5 g LiCl in ddH_2O) onto the electrodes and solidified overnight. No additional current collector was needed.

Characterizations

Transmission electron microscope (TEM) images were performed on a field-emission TEM (Talos F200X, FEI) operating at 200 kV. Scanning electron microscope (SEM) images were performed on FE-SEM (Carl Zeiss NVision 40 integrated with an EDAX system) at an accelerating voltage of 10.0 kV. X-ray photoelectron spectroscopy (XPS) analysis was measured on an ESCALAB MKII X-ray photoelectron spectrometer (VG Co.) with Al Kα X-rays radiation as the X-ray source for excitation. X-ray diffraction (XRD) analysis was carried out on a Rigaku D/Max 2550 X-ray diffractometer using Cu/Kα radiation (35 kV, 200 mA) in the range of 10° — 90° (2θ). Atomic force microscopy (AFM) images were obtained with Veeco Instruments Nanoscope in tapping mode. The samples for AFM measurements were prepared by dropping the diluted colloidal suspension (0.01 mg mL^{-1}) onto a freshly cleaved mica surface and then dried in a vacuum.

Electrochemical measurements

CV, EIS, and GCD analyses were performed on an electrochemical workstation (Biologic VMP3). EIS measurements are performed at open-circuit voltage with frequencies ranging from 100 kHz to 10 mHz.

The gravimetric capacitance (C_g) for the synthesized materials was tested in a three-electrode system in 5 M LiCl, where the counter electrode was Pt plate, and the reference electrode was Ag/AgCl in saturated KCl aqueous solution. The potential window is from −0.8 V to −0.3 V *vs.* Ag/AgCl. The CV profiles were collected at the scan rates of 5, 10, 20, 40, and 80 mV s^{-1} and the GCD profiles are collected at the speeds of 0.5, 1, 2, 5, and 10 A g^{-1}. Cycling tests for NPy-1 and $NbSe_2$ are conducted at 5 A g^{-1} for 10000 cycles.

The assembled supercapacitor was tested in a two-electrode system with the NPy-1 as the anode and MnO_2 as the cathode. The potential window is able to reach up to 1.8 V. The electrochemical performance were measured under potential output window 1.2 V − 1.8 V. The GCD curves are collected at 0.5, 1, 2, 4 and 8 mA cm^{-2} and the CV profiles are scanned at 5, 10, 20, 40, and 80 mV s^{-1}. To test the uniformity of the assembled devices, two devices were connected in series and parallel. Cycling tests were conducted at 6 mA cm^{-2} for 10000 cycles.

The capacitance, in general, was given by the following formula:

$$C = \frac{\int I dt}{\Delta U} \qquad \#1$$

Where C is the capacitance, I is the current, t is the time, ΔU is the applied potential window.

When calculated from the CV profile, the formula can be transformed into:

$$C = \frac{\int I d\frac{U}{v}}{\Delta U} = \frac{\int I dU}{v \Delta U} \qquad \#2$$

Where U is the potential and v is the applied scan rate.

When calculated from the GCD curve, the formula can be simplified into:

$$C = \frac{It}{\Delta U} \qquad \#3$$

Gravimetric capacitance C_g is calculated based on the mass of materials used in the working electrode. Areal capacitance C_a and volumetric capacitance C_v are calculated based on the area or the volume of the device electrodes.

In this work, the electrochemical performance of NPy-1 nanosheets was evaluated by gravimetric capacitance C_g, which is calculated based on the mass load of the material on the working electrode. As for the assembled asymmetric supercapacitor NPy-1//MnO_2, the volumetric capacitance C_v is considered, which is a more critical factor for practical purposes. The area used is the area of the round electrode with a diameter of 16 mm and the volume is calculated based on the total electrode volume excluding the electrolyte, which is the product of the area and the total thickness of both electrodes.

The volumetric power (P, in W cm^{-3}) and energy (E, in Wh cm^{-3}) density of the device were calculated using the following formula:

$$E = 0.5Cv\Delta U^2 \qquad \#4$$

$$P = \frac{E}{\Delta t} \qquad \#5$$

Where Δt is the discharge time.

Supplemental figures and tables

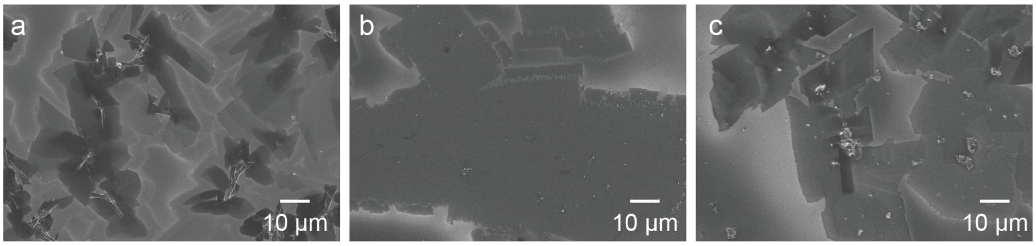

Figure S1 Morphology characterization of NPy-n nanosheets. SEM image of NPy-1 (a), NPy-2 (b) and NPy-3 (c) nanosheets.

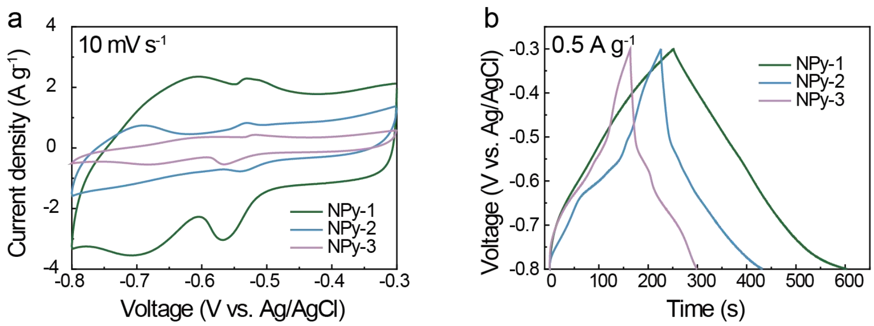

Figure S2 Electrochemical performance of $NbSe_2$@PPy (NPy-x). Cyclic voltammetry (a) with a sweeping rate of 10 mV s^{-1} and galvanostatic charge-discharge profiles (b) at a current density of 0.5 A g^{-1} for NPy-x electrodes in 5 M LiCl. Results show that NPy-1 exhibited the highest capacitance, thus being further investigated.

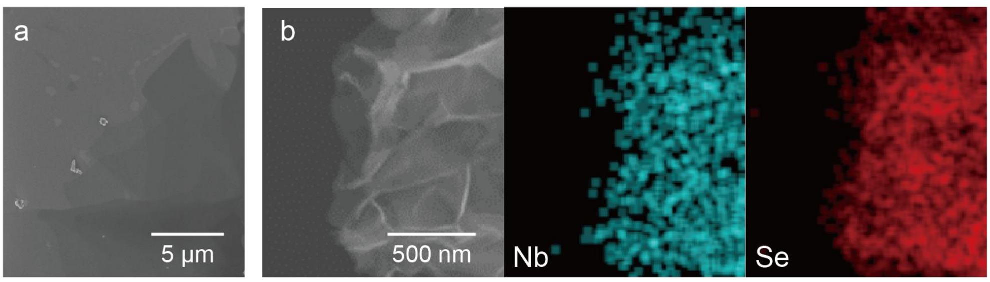

Figure S3 Morphology characterization of $NbSe_2$ nanosheets. SEM image (a) and EDS elemental mapping (b) of $NbSe_2$ nanosheets.

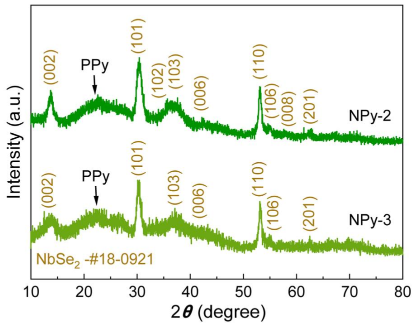

Figure S4 XRD spectra for NPy-2 and NPy-3.

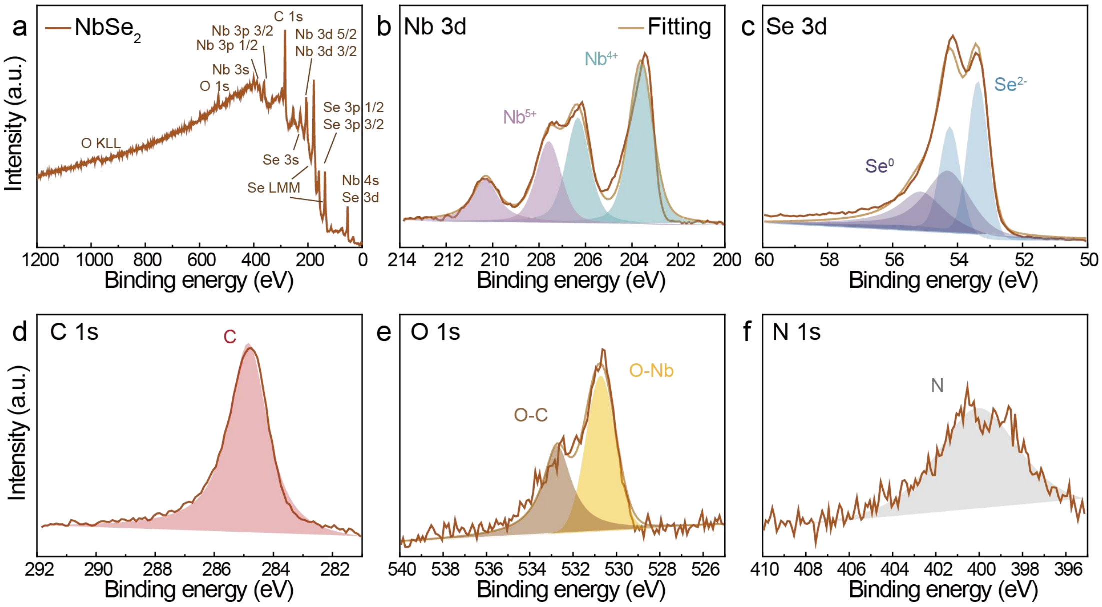

Figure S5 XPS spectra of $NbSe_2$ nanosheets. Full XPS spectrum (a) and high-resolution XPS spectra of Nb 3d, Se 3d, C 1s, O 1s, and N 1s (b-f) for $NbSe_2$ nanosheets.

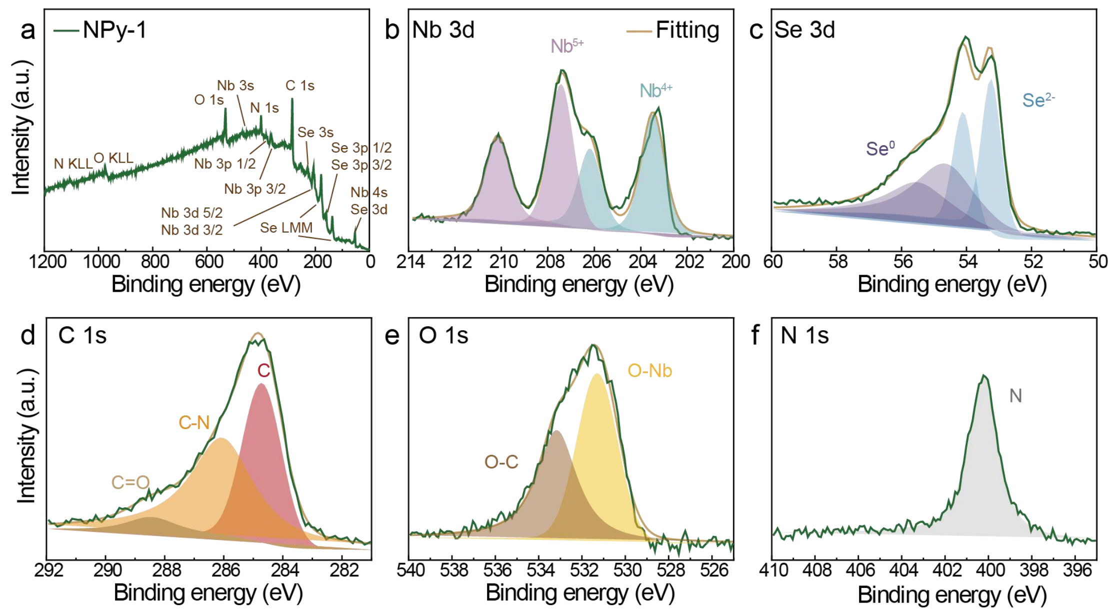

Figure S6 XPS spectra of NPy-1. Full XPS spectrum (a) and high-resolution XPS spectra of Nb 3d, Se 3d, C 1s, O 1s, and N 1s (b-f) for NPy-1.

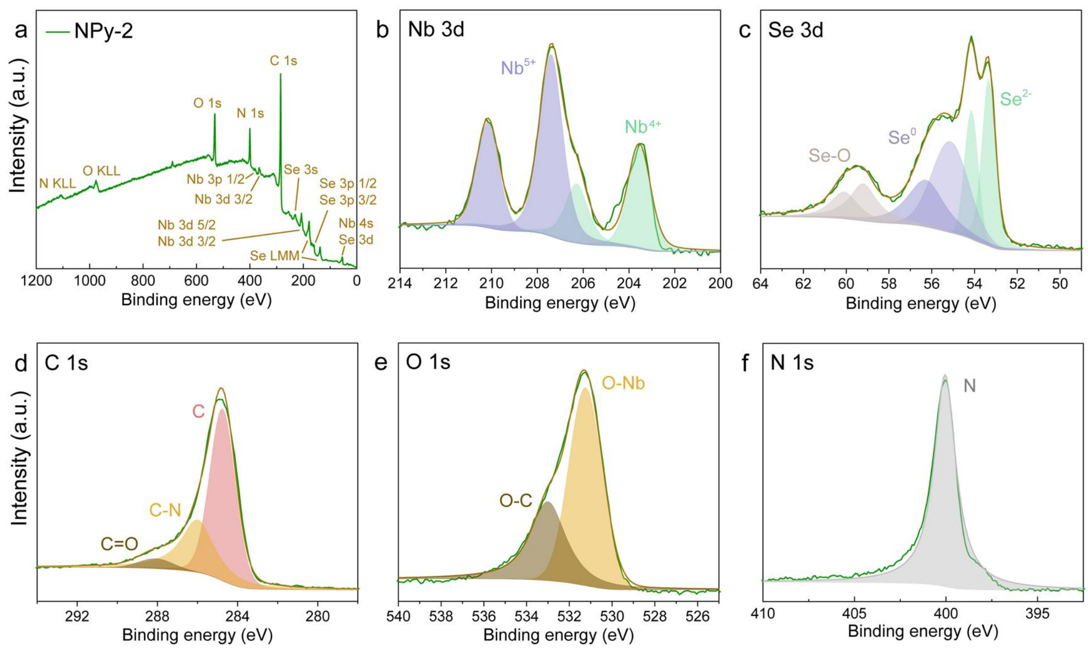

Figure S7 XPS spectra of NPy-2. Full XPS spectrum (a) and high-resolution XPS spectra of Nb 3d, Se 3d, C 1s, O 1s, and N 1s (b-f) for NPy-2.

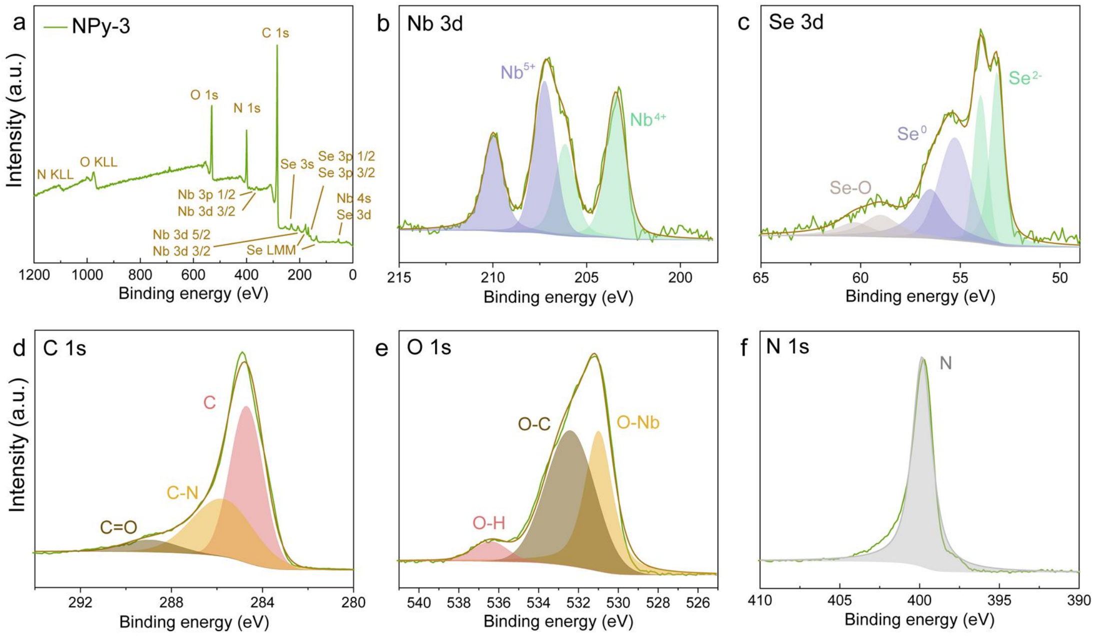

Figure S8 XPS spectra of NPy-3. Full XPS spectrum (a) and high-resolution XPS spectra of Nb 3d, Se 3d, C 1s, O 1s, and N 1s (b-f) for NPy-3.

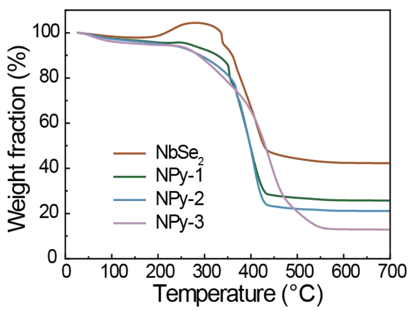

Figure S9 TGA curves of $NbSe_2$ and NPy-x under air atmosphere. The mass ratio of surface PPy to $NbSe_2$ were tuned by the amount of pyrrole added during oxidative polymerization. The mass ratios of $NbSe_2$:PPy are determined to be 1 : 0.64, 1 : 0.97, 1 : 2.3 for NPy-1, NPy-2, NPy-3, respectively.

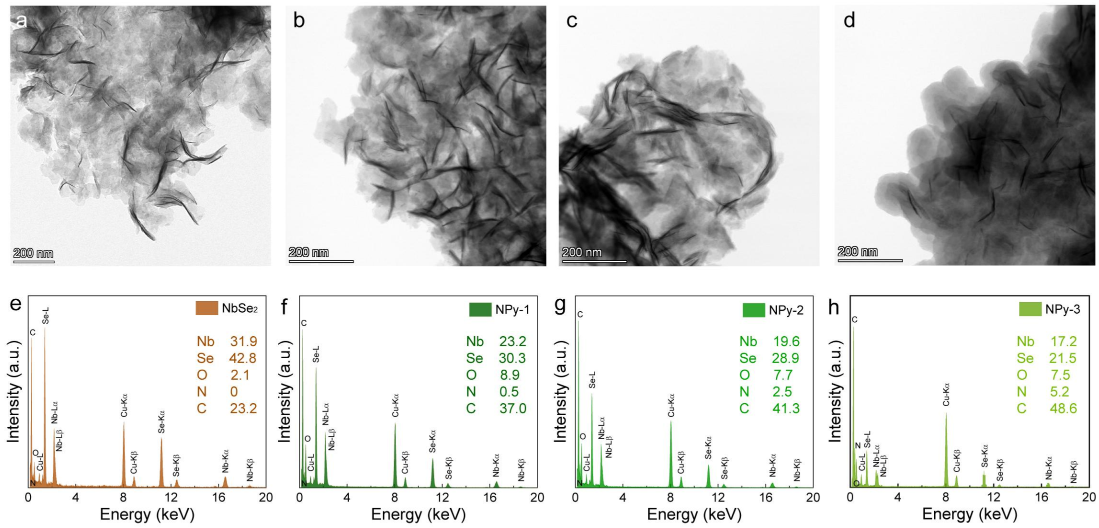

Figure S10 TEM images and EDS spectra of $NbSe_2$ and NPy-x. The mass percents of Nb, Se, O, N, and C elements are determined. The actual content of C element is less than the value measured due to the contribution from the carbon film on copper mesh.

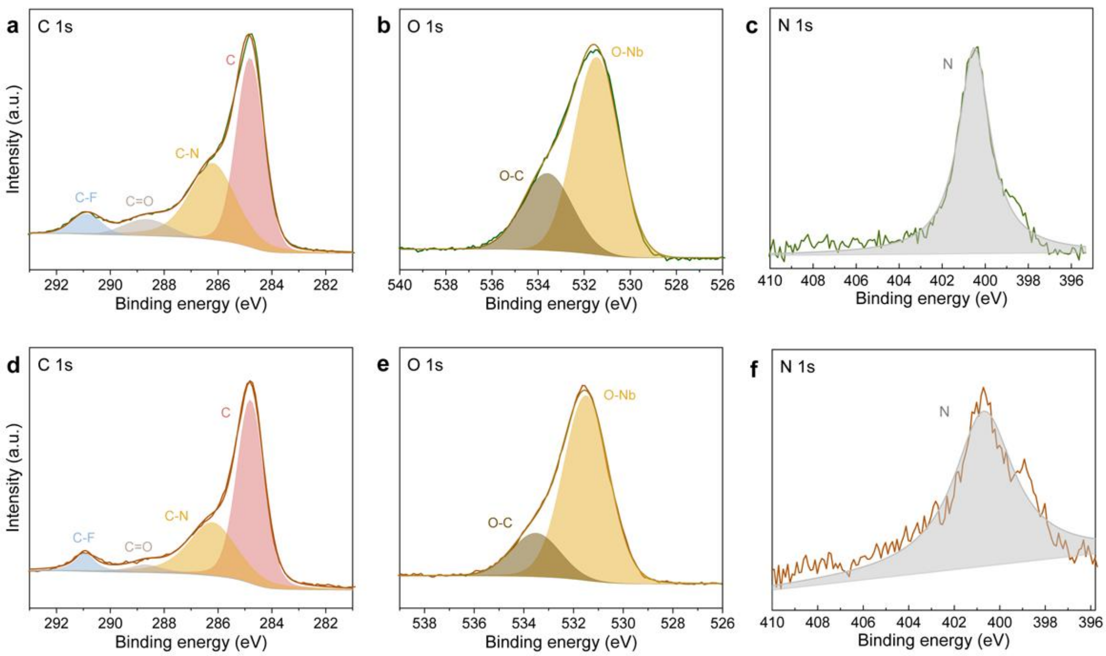

Figure S11 High-resolution XPS spectra of C 1s, O 1s, and N 1s for NPy-1 (a-c) and $NbSe_2$ (d-f) after cycling in three-electrode system.

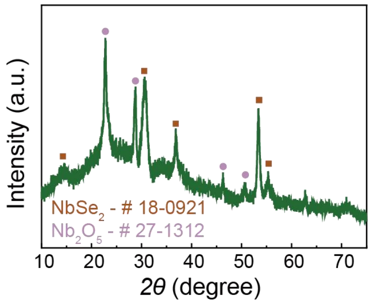

Figure S12 XRD patterns of NPy-1 after cycling in the assembled asymmetric all-solid-state supercapacitor.

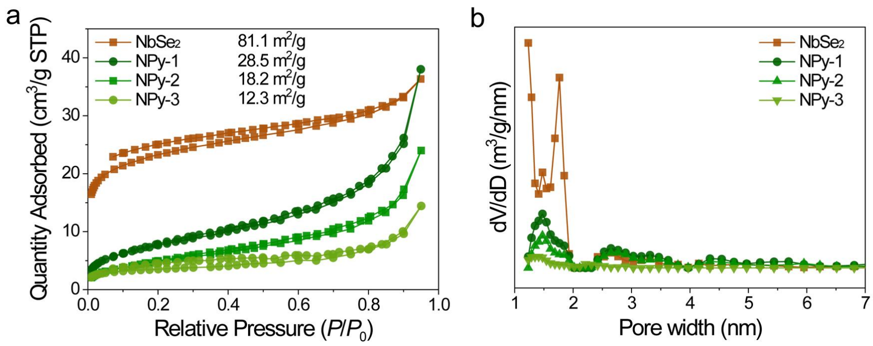

Figure S13 Specific surface area (a) and pore size distribution of $NbSe_2$ and NPy-x nanosheets by density functional theory (DFT) mode

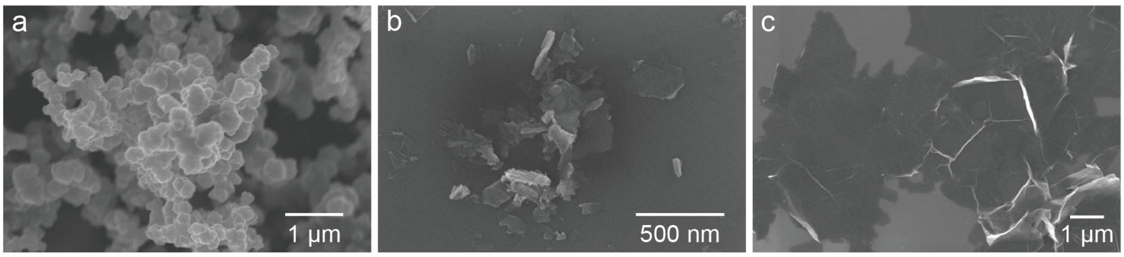

Figure S14 SEM images of synthesized PPy (a), MnO_2 nanosheets (b), and exfoliated graphene (EG) (c).

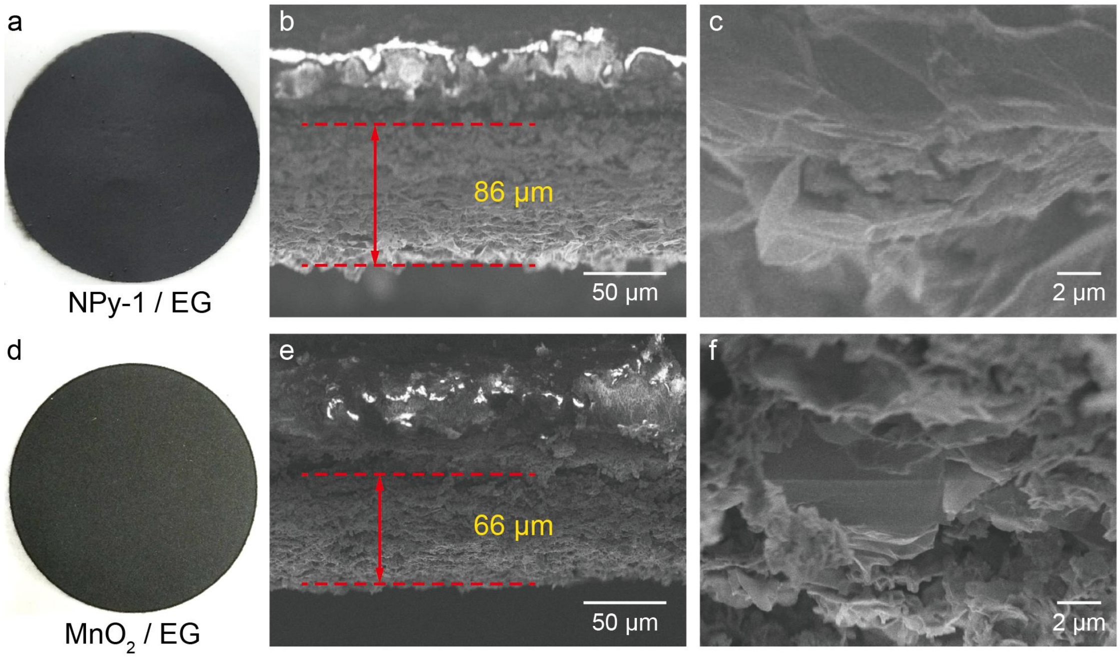

Figure S15 Characterization of the electrode used in the assembled all-solid-state supercapacitor. The photograph (a), low- (b) and high- (c) magnification cross-sectional SEM images of 86 μm thick NPy-1/EG electrode. The photograph (d), low- (e) and high- (f) magnification cross-sectional SEM images of 66 μm thick MnO_2/EG electrode.

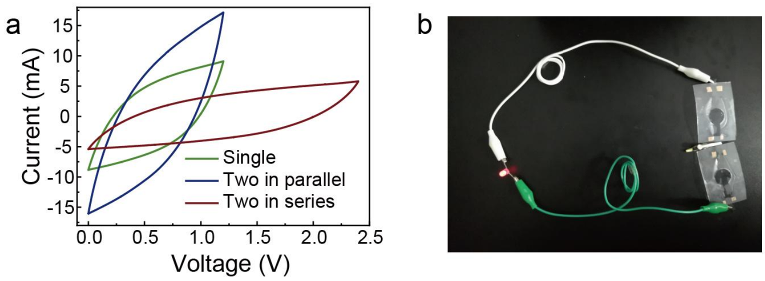

Figure S16 (a) CV curves with the sweeping rate of 50 mV s^{-1} for one device and two devices connected in series and parallel. (b) Two supercapacitors connected in series can light a bulb.

Table S1 Summary of supercapacitor properties for TMD based electrodes.

Material	Capacitance ($F\ g^{-1}$)	Electrolyte	Current density/ Scan rate	Capacitance retention (n cycles)	Reference
NPy-1 ($NbSe_2$@PPy)	394 353	5 M LiCl	5 mV s^{-1}; 0.5 A g^{-1}	97.0% (10000)	This work
1T MoS_2	188	0.5 M K_2SO_4	0.5 A g^{-1}	90% (5000)	Ref. 4
TaS_2	94	PVA/LiCl	0.5 A g^{-1}	92% (4000)	Ref. 5
MoS_2	380	0.5 M Li_2SO_4	5 mV s^{-1}	88% (5000)	Ref. 6
MoS_2/rGO	265	1 M $HClO_4$	10 mV s^{-1}	92% (1000)	Ref. 7
MoS_2/NiS	1373	6 M KOH	0.5 A g^{-1}	93.8% (7000)	Ref. 8
MoS_2/G	272	6 M KOH	5 mV s^{-1}	120% (4000)	Ref. 9
$CeSe_2$	195.6	1 M Na_2SO_3	2 mV s^{-1}	88.4% (4000)	Ref. 10

References

(1) Hu, Z.; Xiao, X.; Jin, H.; Li, T.; Chen, M.; Liang, Z.; Guo, Z.; Li, J.; Wan, J.; Huang, L.; Zhang, Y.; Feng, G.; Zhou, J. Rapid Mass Production of Two-Dimensional Metal Oxides and Hydroxides via the Molten Salts Method. *Nat. Commun.* 2017, **8**, 15630.

(2) Yang, S.; Brüller, S.; Wu, Z. S.; Liu, Z.; Parvez, K.; Dong, R.; Richard, F.; Samorì, P.; Feng, X.; Müllen, K. Organic Radical-Assisted Electrochemical Exfoliation for the Scalable Production of High-Quality Graphene. *J. Am. Chem. Soc.* 2015, **137**, 13927–13932.

(3) Parvez, K.; Wu, Z. S.; Li, R.; Liu, X.; Graf, R.; Feng, X.; Müllen, K. Exfoliation of Graphite into Graphene in Aqueous Solutions of Inorganic Salts. *J. Am. Chem. Soc.* 2014, **136**, 6083–6091.

(4) Acerce, M.; Voiry, D.; Chhowalla, M. Metallic 1T Phase MoS_2 Nanosheets as Supercapacitor Electrode Materials. *Nat. Nanotechnol.* 2015, **10**, 313–318.

(5) Wu, J.; Peng, J.; Yu, Z.; Zhou, Y.; Guo, Y.; Li, Z.; Lin, Y.; Ruan, K.; Wu, C.; Xie, Y. Acid-Assisted Exfoliation toward Metallic Sub-Nanopore TaS_2 Monolayer with High Volumetric Capacitance. *J. Am. Chem. Soc.* 2018, **140**, 493–498.

(6) Geng, X.; Zhang, Y.; Han, Y.; Li, J.; Yang, L.; Benamara, M.; Chen, L.; Zhu, H. Two-Dimensional Water-Coupled Metallic MoS_2 with Nanochannels

for Ultrafast Supercapacitors. *Nano Lett.* 2017, **17**, 1825–1832.

(7) Da Silveira Firmiano, E. G.; Rabelo, A. C.; Dalmaschio, C. J.; Pinheiro, A. N.; Pereira, E. C.; Schreiner, W. H.; Leite, E. R. Supercapacitor Electrodes Obtained by Directly Bonding 2D MoS_2 on Reduced Graphene Oxide. *Adv. Energy Mater.* 2014, **4**, 1301380.

(8) Qin, Q.; Chen, L.; Wei, T.; Liu, X. MoS_2/NiS Yolk–Shell Microsphere-Based Electrodes for Overall Water Splitting and Asymmetric Supercapacitor. *Small* 2019, **15**, 1803639.

(9) Ke, Q.; Zhang, X.; Zang, W.; Elshahawy, A. M.; Hu, Y.; He, Q.; Pennycook, S. J.; Cai, Y.; Wang, J. Strong Charge Transfer at 2H–1T Phase Boundary of MoS_2 for Superb High-Performance Energy Storage. *Small* 2019, **15**, 1900131.

(10) Pandit, B.; Agarwal, A.; Patel, P.; Sankapal, B. R. The Electrochemical Kinetics of Cerium Selenide Nano-Pebbles: The Design of a Device-Grade Symmetric Configured Wide-Potential Flexible Solid-State Supercapacitor. *Nanoscale Adv.* 2021, **3**, 1057–1066.